Nuclear condensation and the equation of state of nuclear matter

J. N. De and S. K. Samaddar
Saha Institute of Nuclear Physics, 1/AF Bidhannagar, Kolkata 700 064, India
(Received 22 May 2007; revised manuscript received 14 August 2007; published 23 October 2007)

The isothermal compression of a dilute nucleonic gas invoking cluster degrees of freedom is studied in an equilibrium statistical model; this clusterized system is found to be more stable than the pure nucleonic system. The equation of state (EoS) of this matter, shows features qualitatively very similar to the one obtained from pure nucleonic gas. In the isothermal compression process, there is a sudden enhancement of clusterization at a transition density rendering features analogous to the gas-liquid phase transition in normal dilute nucleonic matter. Different observables like the caloric curves, heat capacities, isospin distillation, etc are studied in both the models. Possible changes in the observables due to recently indicated medium modifications in the symmetry energy are also investigated.

DOI: 10.1103/PhysRevC.76.044607 PACS number(s): 24.10.Pa, 25.70.Pq, 21.65.+f

I. INTRODUCTION

Nuclei expand with excitation. If the excitation energy per nucleon E^*/A is sufficiently high, the compound nuclear configuration is no longer a stable one and the hot nuclei disassemble into many fragments. This general observation [1–3] from intermediate energy heavy ion collisions has been termed as nuclear multifragmentation. Beyond a certain excitation, the nuclear system is also found to vaporize mostly into nucleon gas [4,5] with all produced fragments having atomic numbers <3. The associated temperature corresponding to this excitation can be identified as the boiling temperature of the fragmenting nucleus.

The study of the correlation of temperature with the total excitation energy obtained from the energetics of the generated fragments generally reveals a plateau [6,7] over an excitation energy range of around 3 MeV $\leqslant E^*/A \leqslant$ 10 MeV. This is reminiscent of the liquid to gas phase transition in a thermodynamic system, understood as a crossover of the denser homogeneous nuclear matter to a continuum of subnuclear densities where nucleons and larger nucleonic clusters coexist in thermal and chemical equilibrium. This basic picture is at the heart of various statistical models [1,3,8] for multifragmentation that have been quite successful in explaining many features of the experimental data.

The laboratory observables on nuclear multifragmentation offer a platform for understanding complex processes in astrophysical context that depend on properties of low density nuclear matter, such as core-collapse supernovae, giant stellar explosions or element formation in explosive nucleosynthesis. Shredded of the minute details, it would be interesting to know what happens to a dilute hot gas of interacting nucleons when compressed isothermally or cooled isochorically. Answers have generally been sought from the statistical mechanics of such an interacting system. Detailed calculations in the relativistic mean-field framework [9] have been done for the EoS of infinite nuclear matter of different neutron-proton concentrations. The main conclusions are (i) the nucleons in the gas phase condense to a bulk liquid phase with which it remains in coexistence over a range of densities, (ii) at constant pressure the gas-liquid phase transition occurs at a constant temperature for the symmetric system ($N = Z$) alluding to a first order phase transition; for the asymmetric systems, however, isobaric transition occurs over a range of temperatures indicating a continuous transition, and (iii) the neutron-proton asymmetry in the gas and liquid phases are in general widely different for asymmetric matter (isospin distillation). Similar conclusions have also been arrived at [10] in a nonrelativistic mean-field model.

The mean-field calculations do not account for fluctuations in the nucleonic degrees of freedom that render it possible for cluster formation from the nucleonic gas. On that account, the method of virial expansion has been found to be quite useful and practical in calculating the EoS of dilute gases [11]. The formal structure of the virial coefficients are self-contained, nonetheless, given an interaction potential, the calculation of higher virials are rather tedious. In quantum statistical mechanics, the second virial coefficient may be expressed in terms of scattering phase shifts. Using the modern language of diagrammatics, the general discussion on virial coefficients becomes very elegant and concise [12,13], but the fact remains that a practical calculation of the virial coefficients beyond the second is an onerous task.

The explicit evaluation of the EoS of the interacting dilute gas from the classical virial (cluster) expansion is very cumbersome, but one thing that transpires clearly from the method is that the interacting gas can be treated as a noninteracting gas of clusters of different sizes [14] in thermodynamic equilibrium. In this backdrop, we study the nuclear EoS of both symmetric and asymmetric matter exploiting the nuclear statistical equilibrium (NSE) model as has been employed in understanding the nuclear multifragmentation data or in exploring nucleosynthesis in the astrophysical scenario [15–17]. Explicit consideration of the interaction between nucleons as is required in the cluster expansion is bypassed in this model; their effect is indirectly borne through the binding energies of the clusters, which are taken as phenomenological inputs.

Recent laboratory experiments [18,19] on nuclear disassembly indicate that the properties of the nuclides describing their binding energies are modified at the subnuclear densities ($\rho \sim \rho_0/3$) they are created in. The symmetry energy,

for example, is reported [20] to be progressively reduced with excitation energy which is attributed to the in-medium modifications of the properties of the hot fragments [21] or their expansion [22,23]. Similarly, the surface properties of the hot fragments are speculated to be modified due to the embedding environment [24]. The highest density that we explore in our calculation is relatively dilute compared to the freeze-out density in which the fragments are formed in laboratory experiments. We therefore do not expect the in-medium modification of the surface energy to play any significant role in the present context. However, modifications in the symmetry energy are considered as they may arise from expansion of the hot fragments.

The paper is organized as follows. In Sec. II, we briefly outline the statistical equilibrium model. The results and discussions are presented in Sec. III and the concluding remarks are given in Sec. IV.

II. THE STATISTICAL EQUILIBRIUM MODEL

We work in the framework of the grand canonical ensemble. Taking the cue from Ursell and Mayer [14], we assume the interacting dilute nucleon gas to be a noninteracting mixture of nucleons and different nucleonic clusters in thermal and chemical equilibrium. For simplicity of terminology, we henceforth term all the species as particles or fragments that include monomers (neutrons and protons) and more complex clusters. The neutron and proton densities are conserved on the average as

$$\begin{aligned} \sum_i N_i \rho_i &= \rho_n, \\ \sum_i Z_i \rho_i &= \rho_p, \end{aligned} \tag{1}$$

where ρ_n and ρ_p are the total neutron and proton densities of the nuclear matter and ρ_i is the number density of the ith fragment species with N_i neutrons and Z_i protons. The sum in Eq. (2) extends over all the cluster species. The fragment number density ρ_i is obtained as

$$\rho_i = \frac{g_i}{h^3} \int n_i(\mathbf{p_i}) d\mathbf{p_i}. \tag{2}$$

Here g_i is the degeneracy factor, $\mathbf{p_i}$ refers to the momentum of the ith fragment species and n_i is the distribution function given by

$$n_i(\mathbf{p_i}) = [\exp{(\varepsilon_i - \mu_i)/T} \pm 1]^{-1}, \tag{3}$$

where

$$\varepsilon_i = \frac{p_i^2}{2m_i} - B_i \tag{4}$$

is the single particle energy of the fragment species, m_i its mass, B_i the ground state binding energy, and T is the temperature of the system. From the condition of chemical equilibrium, one gets for chemical potential μ_i of the species,

$$\mu_i = N_i \mu_n + Z_i \mu_p, \tag{5}$$

where μ_n and μ_p are the chemical potentials of the monomers in chemical equilibrium with the clusters. These are determined iteratively from the conservation conditions given by Eq. (2). The $+(-)$ signs in Eq. (3) refer to fermions (bosons). The density of the fragment species is obtained after momentum integration of the occupation function [Eq. (2)]; for fermions, taking into account the various excited states of the fragment species, it is given by

$$\rho_i = \frac{2}{\sqrt{\pi}\lambda^3} A_i^{3/2} J_{1/2}^{(+)}(\eta_i) \phi_i(T). \tag{6}$$

Here $\phi_i(T)$ is the internal partition function

$$\begin{aligned} \phi_i(T) &= \sum_k g_i^k e^{-E_i^k/T} \\ &= e^{-F_i/T}, \end{aligned} \tag{7}$$

where E_i^k is the internal excitation energy of the ith species for the kth state and F_i is the internal free energy of the cluster measured with respect to its ground state. Fragments with mass $\leqslant 4$ are assumed to have no internal excitation. Similarly, the density of the bosonic fragments is

$$\rho_i = \frac{g_i^0}{V} \frac{1}{\exp(-\eta_i) - 1} + \frac{2}{\sqrt{\pi}\lambda^3} A_i^{3/2} J_{1/2}^{(-)}(\eta_i) \phi_i(T). \tag{8}$$

In Eqs. (6) and (8), $\lambda = \frac{h}{\sqrt{2\pi m T}}$ is the thermal wavelength of a nucleon (m is the nucleon mass, we assume the neutron and proton mass to be the same), $\eta_i = (\mu_i + B_i)/T$, A_i $(= N_i + Z_i)$ is the fragment mass number, and $\phi_i(T)$ is the internal partition function of the excited fragments which reduces to the ground state degeneracy factor g_i^0 in the limit $T \to 0$. The functions $J_n^{(\pm)}$ are the Fermi (Bose) integrals and V is the volume of the system. The explicit form of the integrals is given by

$$J_n^{(\pm)}(\eta) = \int_0^\infty \frac{x^n}{\exp(x - \eta) \pm 1} dx. \tag{9}$$

The first term in Eq. (8) arises from Bose condensation which we neglect in subsequent calculations as it turns out to be very insignificant in the present context. For the ground state binding energy of the fragments, we take recourse to the recently proposed mass formula by Danielewicz [25]. We have also used the Myers-Swiatecki [26] mass formula, but many nuclear EoS properties investigated with both mass formulas look indistinguishable. We therefore report calculations with the Danielewicz mass formula. In this model, the binding energy of a chargeless nucleus is

$$B_i = a_v A_i - \sigma(X_i, T = 0) A_i^{2/3} - \alpha \left(\frac{N_i - Z_i}{A_i} \right)^2 A_i + \delta. \tag{10}$$

For monomers, B_i is zero. Since the fragments are formed out of chargeless infinite nuclear matter, the Coulomb term has been dropped. In Eq. (10), the first term is the volume term with volume energy coefficient $a_v = 15.6163$ MeV, $\sigma(X, T)$ is the surface energy coefficient and α is the volume symmetry energy coefficient, taken as 32.6655 MeV. The temperature

and asymmetry ($X = (N - Z)/A$) dependent surface energy coefficient is [27]

$$\sigma(X,T) = [\sigma(X=0,T=0) - a_s X^2] \times \left[1 + \frac{3}{2}\frac{T}{T_c}\right]\left[1 - \frac{T}{T_c}\right]^{3/2}, \quad (11)$$

with $\sigma(0,0) = 17.9878$ MeV. The surface symmetry energy coefficient a_s is given by $a_s = (\alpha^2/\beta)/(1 + \alpha/\beta A_i^{-1/3})$ with $\beta = 13.6106$ MeV. The critical temperature of symmetric nuclear matter T_c is taken to be 14.61 MeV. It pertains to the SkM* effective interaction [28] which we use in subsequent calculations. The last term in Eq. (10) is due to pairing which is zero for odd-even nuclides and is equal to $\delta = \pm a_p/\sqrt{A_i}$ for even-even or odd-odd nuclei. For ground state, the value of $a_p = 10.8714$ MeV; as pairing vanishes at above $T \sim 1$ MeV, it is taken to be zero for the NSE calculations reported here. For fragment mass $A_i > 4$, Eq. (10) is employed for calculation of binding energies. For fragments with $A_i \leqslant 4$, they are calculated by subtracting the Coulomb contribution from the experimental binding energies.

The free energy F_i is obtained in the Fermi gas approximation where the volume excitation energy is $a_i T^2$ and the volume entropy $S_i^{\rm vol}$ is $2a_i T$ with a_i, the level density parameter of the ith species being taken as $a_i = A_i/16$. Then we have

$$F_i = [\sigma(X_i,T) - \sigma(X_i, T=0)]A_i^{2/3} - a_i T^2, \quad (12)$$

where the first term is the excess surface free energy due to excitation and is designated as $F_i^{\rm surf}$. The excitation energy per nucleon of the disassembled system is then given by

$$E^*/A = \left(\sum_i \rho_i E_i(T) + \frac{3}{2}\sum_i \rho_i T\right) \Big/ \sum_i \rho_i A_i, \quad (13)$$

where the internal excitation $E_i(T)$ of the ith species is

$$E_i(T) = F_i + T\left(S_i^{\rm vol} + S_i^{\rm surf}\right). \quad (14)$$

The second term in the numerator of Eq. (13) is the kinetic energy density for the center of mass motion of the particles. Here we have used the classical equipartition theorem which is a very good approximation to the quantal result for the dilute system. The surface entropy $S_i^{\rm surf}$ is obtained from $S_i^{\rm surf} = -\partial F_i^{\rm surf}/\partial T$. In addition to the surface and volume terms, the total entropy has a contribution $S_i^{\rm tran}$ from the translational motion of the center of mass of the fragments. The total entropy per nucleon generated from the disassembled nuclear matter is then

$$S/A = \sum_i \rho_i \left(S_i^{\rm surf} + S_i^{\rm vol} + S_i^{\rm tran}\right) \Big/ \sum_i \rho_i A_i, \quad (15)$$

where the translational entropy is taken as [29]

$$S_i^{\rm tran} = \frac{5}{2} + \ln\left(g_i \frac{A_i^{3/2}}{\rho_i \lambda^3}\right). \quad (16)$$

In Eq. (16), for the degeneracy factor g_i, the experimental ground state degeneracy is taken for light fragments ($A \leqslant 16$), otherwise, it is taken to be two for fermions and one for bosons.

The pressure is calculated from the total free energy F as $P = -\partial F/\partial V$ which comes out as

$$P = \sum_i \rho_i T, \quad (17)$$

the sum of the partial pressures of a mixture of noninteracting particles consisting of clusters and monomers. The total multiplicity is $M = \sum_i \rho_i V$.

The quantum distribution function approaches the classical one when $\eta_i = (\mu_i + B_i)/T \ll 0$. In that case, $J_{1/2}^{(\pm)}(\eta) \to \frac{\sqrt{\pi}}{2} e^{\eta}$ and then

$$\rho_i = \frac{A_i^{3/2}}{\lambda^3} e^{\eta_i} \phi_i(T). \quad (18)$$

In the range of densities and temperatures we explore in the present work, this condition is mostly satisfied. Examination of Eqs. (17) and (18) shows that the pressure and the density can be written in the form

$$P = T\sum_i \frac{1}{\lambda^3} d_i (z_n)^{N_i} (z_p)^{Z_i}, \quad (19)$$

$$\rho = \sum_i \rho_i A_i = \sum_i \frac{A_i}{\lambda^3} d_i (z_n)^{N_i} (z_p)^{Z_i}, \quad (20)$$

with fugacity $z_{n,p} = e^{\mu_{n,p}/T}$ and $d_i = A_i^{3/2} e^{B_i/T}\phi_i(T)$. For a one component system, one readily sees that the above equations have the structure analogous to the ones obtained from cluster expansion [11]

$$P/T = \frac{1}{\lambda^3}\sum_i b_i z^i, \quad (21)$$

$$\rho = \frac{1}{\lambda^3}\sum_i i b_i z^i, \quad (22)$$

with $z = e^{\mu/T}$ ($\mu_n = \mu_p = \mu$) and b_i is the cluster integral. In cluster expansion, information on the two-body interaction is contained in the cluster integral b_i, similarly in the NSE model, this information is embedded as binding energy in d_i. The two models are not equivalent; an i-particle cluster in the cluster expansion includes both bound and continuum states and the b_i's in this expansion can be negative [14]. The d_i's in the NSE model are, however, always positive, they include only a variety of bound states.

III. RESULTS AND DISCUSSIONS

In the mean-field models of gas-liquid phase transition [9,10], the hot dilute nuclear gas is assumed to consist only of monomers. With isothermal compression or isochoric cooling, a critical stage is reached when there is a sudden onset of bulk liquid formation in coexistence with the monomers. This is the condensation point (the gas-liquid transition). We refer to this model as NM model. In the NSE model, even at very low density, in addition to monomers, the system may contain dimers and lighter clusters, though in

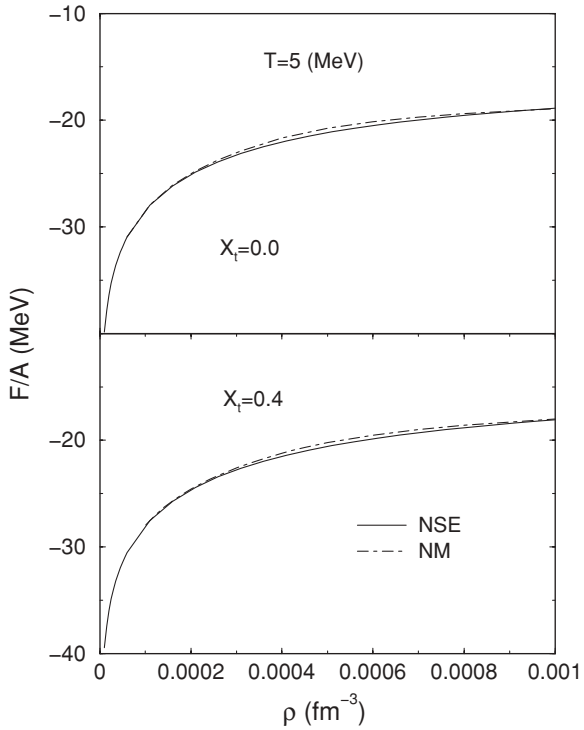

FIG. 1. The free energy per nucleon shown as a function of density for symmetric (upper panel) and asymmetric (lower panel) nuclear matter at a temperature $T = 5$ MeV. The full and dash lines refer to the NSE and NM models, respectively.

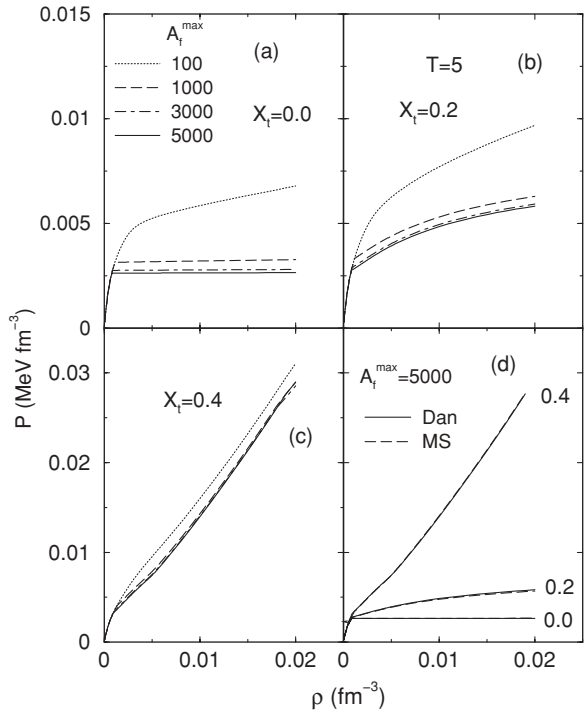

FIG. 2. The sensitivity of the isotherm on the choice of $A_f^{\max}$ (see text) shown at $T = 5$ MeV for symmetric and asymmetric nuclear matter in (a), (b), and (c). (d) shows the dependence of isotherm on asymmetry with Danielewicz (Dan) and Myers-Swiatecki (MS) mass formula.

macroscopically very insignificant amount. With compression or cooling, the clusters grow in size which becomes critical around the condensation point. Thermodynamically, this is more favorable compared to the pure monomeric picture. This is evident from a comparison of the free energy per nucleon which is displayed in Fig. 1, calculated at a temperature $T = 5$ MeV, with both the NSE and NM models, for symmetric and asymmetric nuclear matter. Details of the calculations in the NSE model are postponed till the next paragraph. It is seen that at very low density when cluster formation is insignificant, the two free energies are indistinguishable. We restrict this calculation in a relatively dilute regime where interactions in the NM model can be ignored.

In infinite matter, the maximum cluster size $A_f^{\max}$ can, in principle, be infinite. Numerical calculations necessitate the restriction of $A_f^{\max}$ to a finite number. The thermodynamic observables are sensitive to the choice of $A_f^{\max}$. The results, however, tend to converge with increasing $A_f^{\max}$ which is displayed in Fig. 2 for isotherms drawn at $T = 5$ MeV for nuclear matter of different asymmetries (X_t). In panels (a), (b), and (c), the isotherms are drawn for asymmetries $X_t = 0.0$, 0.2, and 0.4, respectively, for different $A_f^{\max}$ and it seen that they tend to converge at $A_f^{\max} \sim 5000$, the convergence being faster with increasing asymmetry. The results in Fig. 1 and all the subsequent calculations reported are performed with $A_f^{\max} = 5000$ unless otherwise mentioned. The two-component nature of the system allows formation of asymmetric fragments for even symmetric nuclear matter ($X_t = 0.0$). With the neglect of the difference between the neutron and proton masses, all the observables in symmetric nuclear matter are invariant with respect to interchange of neutron and proton and hence the system is effectively a one-component system. Absence of Coulomb interaction helps in the formation of fragments with lower asymmetry and therefore consideration of fragments with asymmetry in the range $-0.3 \leqslant X_i \leqslant 0.3$ suffices, even for very asymmetric nuclear matter. To facilitate the comparison of the dependence of the isotherms on the asymmetry of nuclear matter in the NSE model, they are shown in panel (d) of the figure at $T = 5$ MeV, for $X_t = 0.0$, 0.2, and 0.4. Unlike the NM model, a sharp condensation point cannot be defined in the NSE model, however, a break in the $P - \rho$ curve is apparent when larger clusters start to form suddenly, the break being sharper with lesser asymmetry. In this panel, calculations with the Myers-Swiatecki mass formula are also displayed; they are practically identical with the ones performed with the Danielewicz mass formula. The evolution of the isotherms with asymmetry in the NSE model is very similar to those [9] obtained from the NM model; for symmetric nuclear matter, the condensation occurs practically at constant pressure whereas for the asymmetric systems, the pressure increases. Such a behavior with clusterization has also been reported earlier [30]. The chemical equilibrium conditions coupled with the conservation of the nucleon number and isospin underlies this behavior.

On a somewhat formal footing, this is understood by exploiting Eq. (20). For simplicity, we consider a one-component system, extension to two-component system is

straightforward. The population of a cluster of size i in the one-component system can be written as

$$\omega_i = \frac{V}{\lambda^3} c_i (b_0 z)^i, \tag{23}$$

with $c_i = i^{3/2} \exp(-\sigma(T) i^{2/3})$ and $b_0 = \exp(a_v + \frac{T^2}{16})$. As the i-dependence of c_i is relatively weak compared to $(b_0 z)^i$, when $i \gg 1$ and $z < b_0^{-1}$, ω_i is practically zero and one can consider condensation insignificant in a macroscopic sense. As z increases and passes through the critical value, the density given by the sum in Eq. (22) shoots up very fast. In other words, the density is a very sensitive function of z or the chemical potential, which thus shows a near constancy in the condensation region. The pressure is an explicit function of z and T and depends on the density only in a thermodynamically negligible manner and thus shows the same features as the chemical potential. For asymmetric systems, say, with neutron excess, the population of clusters with N_i neutrons and Z_i protons is

$$\omega_i = \frac{V}{\lambda^3} c_i (b_{0,n} z_n)^{N_i} (b_{0,p} z_p)^{Z_i}. \tag{24}$$

Formation of symmetric fragments is more probable from binding energy considerations, hence as larger fragments start to form, free neutrons become more in excess over protons (isospin distillation) and the z_n starts to increase and z_p decreases. This extra degree of freedom keeps the situation more subtle in asymmetric matter resulting in increase of pressure with density in the transition region.

In Fig. 3, the nucleon fraction constituting the gas phase or the liquid phase as a function of nuclear density is displayed at $T = 2$ and 5 MeV for symmetric nuclear matter. The monomers are considered as gas while the rest (dimers and larger clusters) constitute the liquid part. The baryon fraction R is defined as $R_{l,g} = A_{l,g}/(A_l + A_g)$ where l, g stand for the liquid and gas phases, $A_{l,g}$ being the nucleon number in the respective phases. With increasing density, the liquid fraction R_l initially rises very fast and then gradually approaches unity. The behavior of the gas fraction is just the opposite. In panels (a) and (b) of this figure, the effect of the choice of $A_f^{\max}$ at the two temperatures is shown. It is seen that the choice of the maximum cluster size we made for our calculations is satisfactory. In panels (c) and (d), the liquid and gas fractions in the NSE and the NM models are compared at the two temperatures. They are not too different; at high densities, these fractions tend to merge in these model calculations.

In the upper panel of Fig. 4, A_l/A_g, the ratio of the numbers of nucleons in the liquid to gas phase as a function of density for asymmetric nuclear matter ($X_t = 0.4$) in the NSE and the NM models at $T = 5$ MeV are compared. As with symmetric nuclear matter, here also there is not much significant difference in the results from the two models. The intersection of the dashed line with the abscissa defines the condensation point in the NM model below which there is no liquid; in the NSE model, however, the liquid phase starts at a lower density as there can still be some light clusters in the dilute matter. The lower panel in the figure displays the isotherms for the said system. The overall behavior of the pressure with density in both the models are the same, the

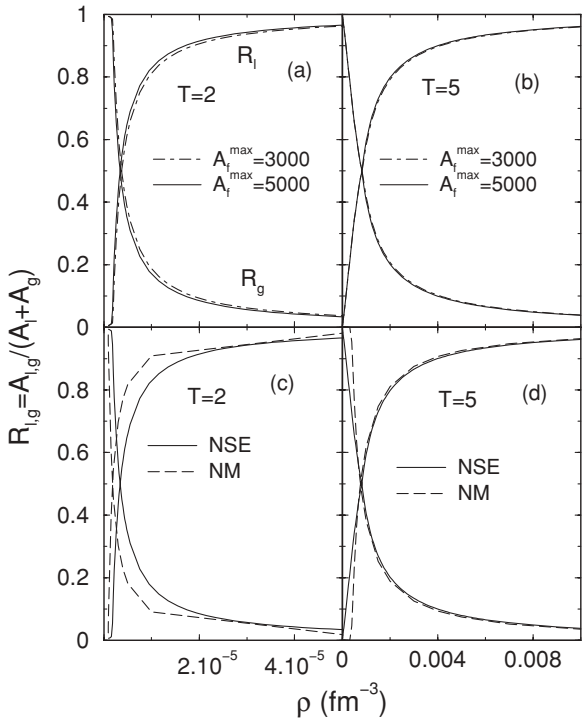

FIG. 3. Dependence of nucleon fraction as a function of density in the liquid (R_l) and in the gas (R_g) phase on $A_f^{\max}$ and temperature displayed in (a) and (b) in the NSE model. The model dependence of the nucleon fractions are shown in (c) and (d) at two temperatures. All the calculations are for symmetric nuclear matter.

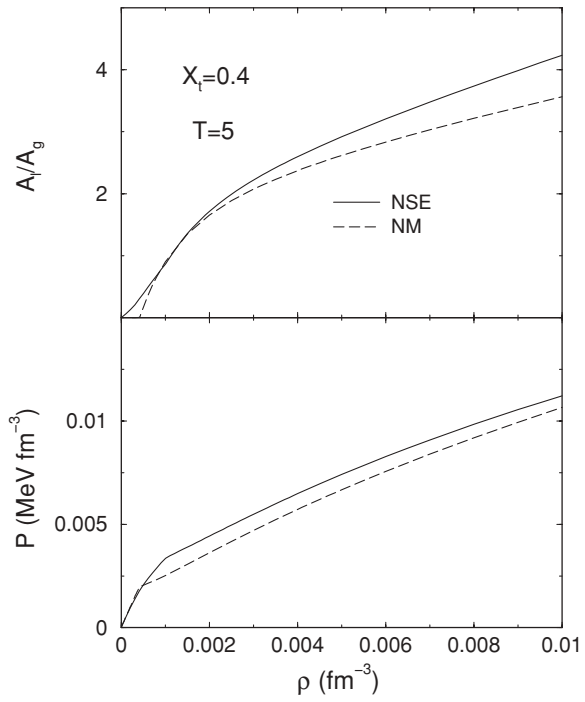

FIG. 4. In the upper panel, the ratio of nucleons in the liquid to that in the gas phase as a function of density at $T = 5$ MeV is compared in the NM and NSE models for asymmetric nuclear matter ($X_t = 0.4$). The lower panel shows the comparison of the isotherms for the same system in the two models.

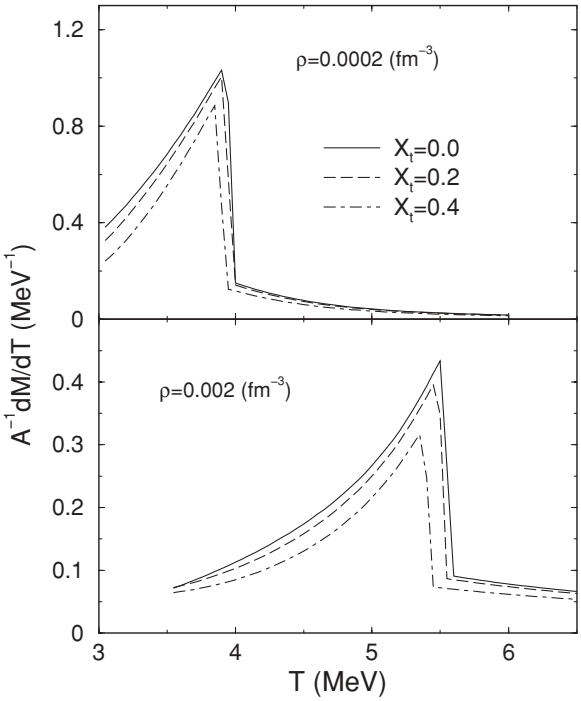

FIG. 5. Multiplicity growth in isochoric cooling shown at two densities for different asymmetries.

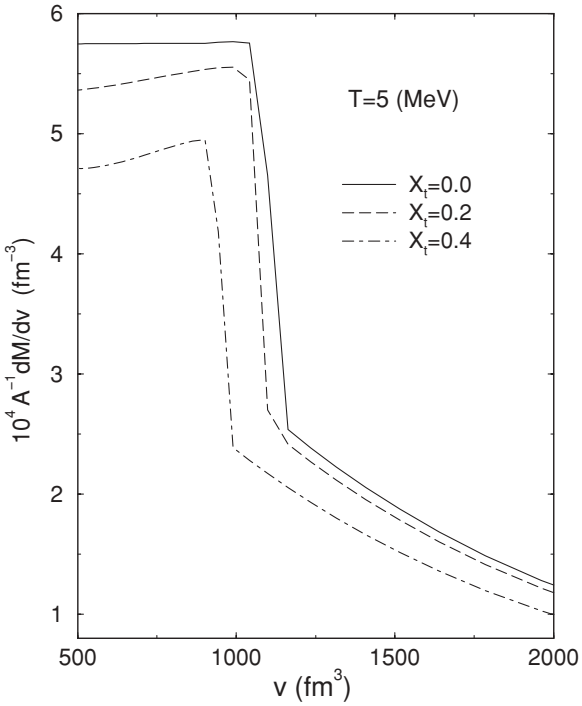

FIG. 6. Multiplicity growth in isothermal compression at $T = 5$ MeV shown for different asymmetries.

pressure increases with density beyond the condensation point as opposed to symmetric nuclear matter. The pressure is seen to be somewhat lower in the NM model. This is understandable. In the NM model, the pressure in the coexistence region is given either by the liquid pressure or the gas pressure ($P = P_l = P_g$) whereas in the NSE model, the sum of the two pressures ($P = P_l + P_g$) has to be counted.

In Fig. 5, the response of the dilute nuclear systems of different neutron and proton concentration to cluster formation on isochoric cooling is displayed. The upper and lower panels correspond to densities $\rho = 0.0002$ and 0.002 fm^{-3}. The rate of change of the total multiplicity M per baryon with temperature ($A^{-1}dM/dT$, A refers to the total number of nucleons in the system) is taken to be a measure of this response. At higher T, the system is mostly in the monomeric phase. At a particular density, as the system cools down, clusters start to form and at a particular temperature, there is a sudden growth of cluster formation. This temperature is the condensation temperature which we refer to as the boiling temperature T_b corresponding to this density. As the system is cooled further, the multiplicity decreases because of the formation of larger clusters at the cost of smaller ones which is reflected in the reduction of dM/dT. The boiling temperature is found to be rather insensitive to the neutron-proton asymmetry, there is a nominal decrease in T_b with X_t. The decrease in boiling temperature with decreasing density is more marked.

For dilute matter, the total multiplicity M ($=A$ in the limit of large specific volume $v = 1/\rho$) decreases with isothermal compression. This is shown in Fig. 6 where we display dM/dv, the rate of change of multiplicity with specific volume as a function of v, at a temperature $T = 5$ MeV for different values of X_t. The multiplicity M always decreases in isothermal compression, hence dM/dv is always positive. The discontinuity in dM/dv indicates the suddenness in cluster formation at the condensation point. For symmetric matter, the constancy in dM/dv below condensation volume is a reflection of the constancy of pressure in the transition region. For asymmetric matter, similarly, the fall of dM/dv is indicative of the increase of pressure with density in this region.

In the upper panel of Fig. 7, the caloric curve at a constant density ($\rho = 0.002$ fm^{-3}) for a representative asymmetric system with $X_t = 0.2$ is displayed. The full and dash lines refer to the NSE and the NM models, respectively. Comparison of the two curves shows that at the same excitation energy, the temperature in the NSE model is lower because there is some energy locked up in the creation of surfaces of the clusters. Both the caloric curves have a characteristic plateau in temperature; this signals a liquid-gas type phase transition which is more apparent from the peaked structure of the derivative of the caloric curve, namely, the heat capacity per baryon c_v which is displayed in the lower panel of the figure.

The caloric curves for asymmetric nuclear matter ($X_t = 0.2$) at constant pressures of $P = 0.002$ and 0.02 MeV fm^{-3} are shown in the upper panel of Fig. 8. In both the NSE and NM models, it is seen that the temperature remains nearly constant over a broad excitation energy interval. The corresponding heat capacity per baryon c_p shows very sharp peaks as can be seen from the lower panel of the figure. At high pressure, in both models, the transition temperature is higher; the NSE model shows a lower transition temperature compared to that in the NM model due to reasons as explained in the preceding paragraph. The corresponding entropies per

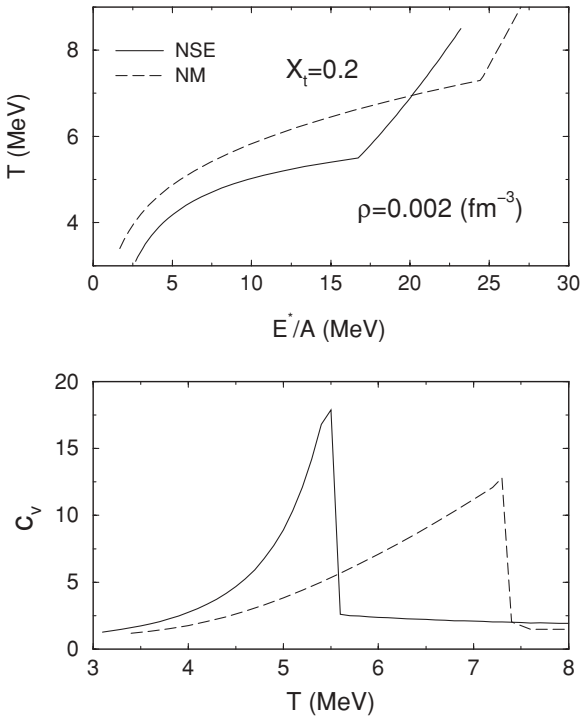

FIG. 7. In the upper panel, caloric curves at constant volume in the NM and NSE models for asymmetric nuclear matter with $X_t = 0.2$ are shown. The corresponding specific heat per nucleon c_v is shown in the lower panel.

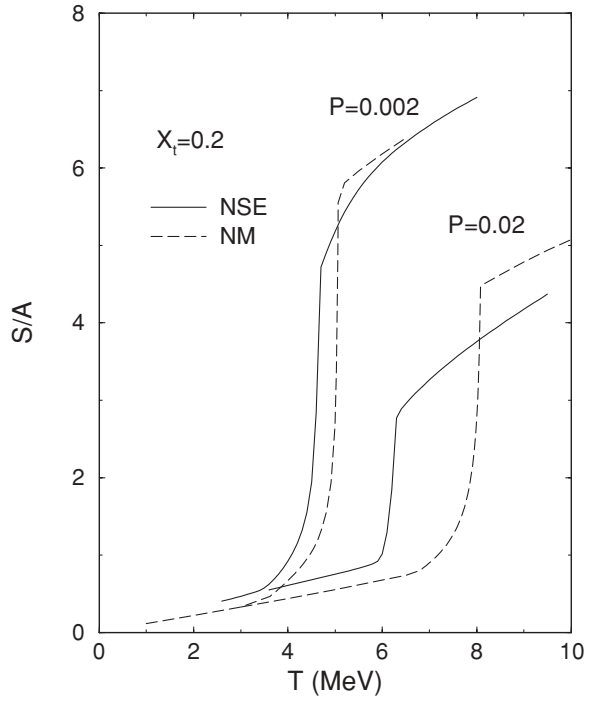

FIG. 9. Evolution of entropy per nucleon with temperature at two different pressures as marked calculated in the NM and NSE models for asymmetric nuclear matter with $X_t = 0.2$.

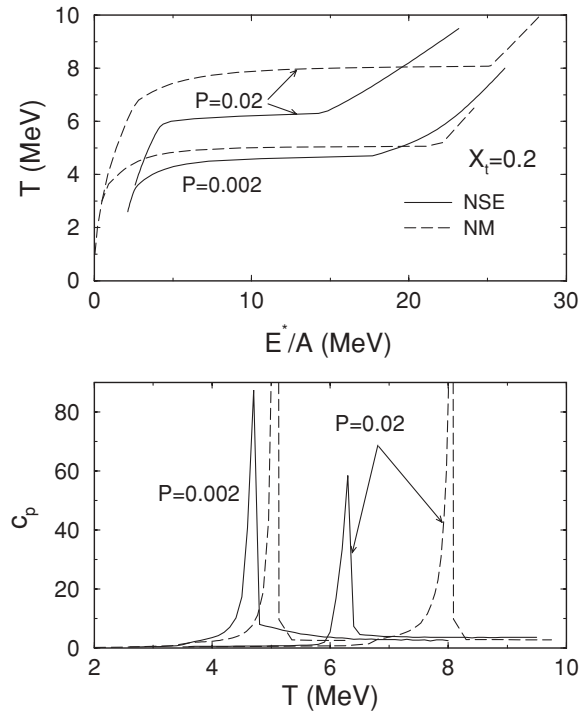

FIG. 8. Caloric curves at two different pressures as marked are shown in the NM and NSE models for asymmetric nuclear matter ($X_t = 0.2$). The corresponding heat capacity c_p per nucleon is shown in the lower panel.

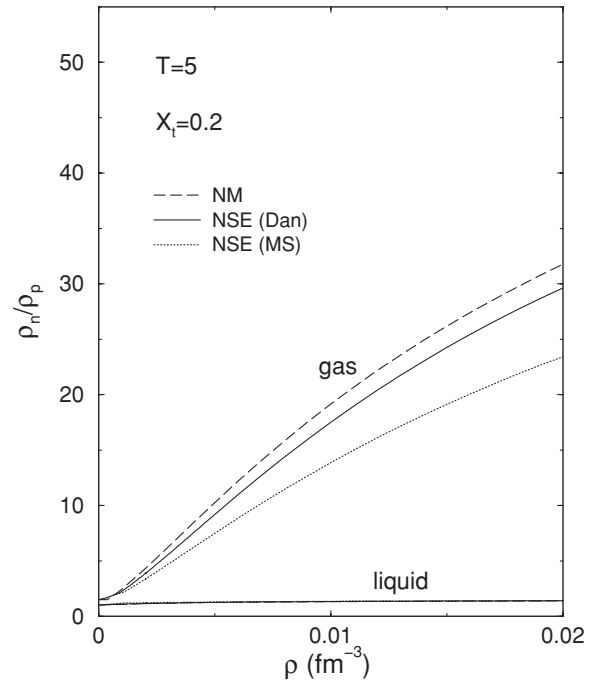

FIG. 10. Evolution of neutron to proton density ratio with isothermal compression at $T = 5$ MeV in the liquid and gas phases for asymmetric nuclear matter ($X_t = 0.2$) calculated in the two models. Calculations in the NSE model have been performed with both Danielewicz (Dan) and Myers-Swiatecki (MS) mass formulas.

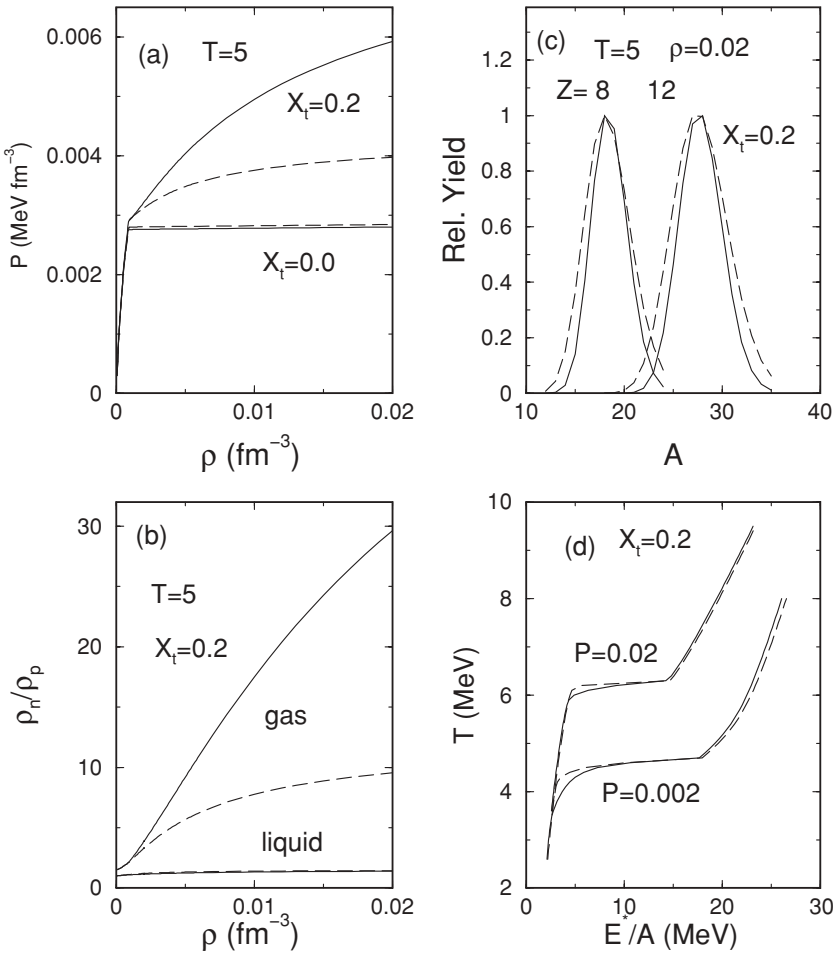

FIG. 11. The effect of symmetry energy on a few observables at $T = 5$ MeV. The full and dashed lines correspond to calculations with the original ground state value and a value reduced by 40% for the symmetry energy in Danielewicz mass formula, respectively. The isotherms, neutron to proton ratio in the liquid and gas phases, isotopic distributions and caloric curves at constant pressure are shown in (a)–(d), respectively. For details, see text.

nucleon S/A as a function of temperature are displayed in Fig. 9. Near the transition temperature, a sharp rise in the entropies can be noted. It may be pointed out that for symmetric nuclear matter, the liquid-gas type phase transition occurs at a constant temperature resulting in a singularity in c_p and a discontinuity in the entropy.

Symmetric cluster formation is more favorable from binding energy considerations. In asymmetric, say, neutron-rich nuclear matter, the monomers left after cluster formation would therefore be richer in neutrons with increase in density. This distillation in isospin is also found in the NM model where from thermodynamic equilibrium conditions, the liquid in the coexistence region tends to become symmetric making the gas phase richer in neutrons with increasing liquid phase. The neutron-proton density ratio ρ_n/ρ_p in the gas and liquid (clusters in the NSE model) in both the models are displayed in Fig. 10. For the liquid phase, this ratio varies from $\sim$1.0 at low density to $\sim$1.5 at higher density (which is the value of the ratio for asymmetry $X_t = 0.2$) and is practically indistinguishable in the two models. However, in the gas phase, there is a dramatic increase in the neutron number over the proton number beyond the transition density; this is more pronounced in the NSE model. Calculations in the NSE model with the Myers-Swiatecki mass formula is also shown in the figure. Though the inclusive observables (like $P - \rho$ correlation) are nearly indistinguishable, isospin distillation shows marked differences between the two mass formulas used. Lesser isospin distillation in the Myers-Swiatecki mass formula is a reflection of its smaller asymmetry energy coefficient compared to that in the Danielewicz formula.

As mentioned in the introduction, analysis of recent experimental data indicates a progressive reduction of the symmetry energy coefficient with the excitation energy of the disassembled system. In the analysis with the SMM multifragmentation model, the freeze-out density is $\sim\rho_0/3$ (where ρ_0 is the normal nuclear matter density), but the nuclear interaction between the produced fragments is neglected which tentatively shows up as in-medium correction to the symmetry energy. Moreover, the possible expansion of the hot fragments is likely to reduce the symmetry energy. In our present context, since we explore from the very dilute density regime to $\rho \sim \rho_0/8$, we do not expect the in-medium corrections to be significant, however, the expansion of the hot fragments might weaken the symmetry energy. *Ab initio* calculations of these effects on symmetry energy are difficult, however, to have a feel how the reduced symmetry energy affects the nuclear observables, we have also performed calculations with symmetry energy reduced by 40% at $T = 5$ MeV. The corresponding results are displayed in Fig. 11. The full lines correspond to the regular system (i.e., the system with the normal value of the symmetry energy coefficient) and the dashed lines to the one with the reduced value of the symmetry

energy in all the panels. In panel (a) of this figure, the nuclear EoS ($P - \rho$ correlation) for both symmetric and asymmetric ($X_t = 0.2$) nuclear matter are shown. Reduction of the symmetry energy coefficient increases the binding energy of the asymmetric fragments and the chemical potential decreases; the increased binding energy tends to reduce the total multiplicity by producing heavy fragments whereas the role of the chemical potential is opposite. A delicate interplay of these two effects is manifested in a very little increase of pressure with reduction of symmetry energy coefficient in case of symmetric matter. This interplay, however, has a different role in case of nuclear matter with sizable asymmetry. For asymmetric matter with reduction in the symmetry energy, more neutrons can be accommodated in relatively heavier fragments and the neutron gas is depleted with reduction of the total multiplicity and hence the pressure. Inspection shows that the results for an asymmetric matter with a reduced symmetry energy coefficient are similar to those of regular system of effectively lower asymmetry.

In panel (b), the neutron-proton density ratio in the liquid and gas phase as a function of density for $X_t = 0.2$ is displayed for both normal and reduced symmetry energies. In the liquid phase, the two results are very close; in the gas phase, as already mentioned, the neutron multiplicity gets depleted and isospin distillation becomes weaker with reduction in symmetry energy. In panel (c), the isospin distribution for nuclei with $Z = 8$ and 12 are compared for both the symmetry energies at a density $\rho = 0.02\ \mathrm{fm}^{-3}$ for $X_t = 0.2$. As expected, the distribution gets wider with decrease in the symmetry energy. In panel (d), the caloric curves at constant pressures $P = 0.002$ and 0.02 MeV fm^{-3} are displayed. The caloric curves are found to be rather insensitive to the variation in the symmetry energy coefficient.

IV. CONCLUDING REMARKS

The equation of state of symmetric and asymmetric dilute nuclear matter and its various thermodynamic properties are studied in the nuclear statistical equilibrium model and compared with those obtained from the conventional mean-field model of nuclear matter. The expressions for the pressure and density in the NSE model have the same structure as those obtained from the method of cluster expansion though the information content in the expansion coefficients is somewhat different. The clusterized matter is more stable than the bulk nuclear matter. The qualitative behavior of the warm dilute matter toward compression or cooling is the same in both the models. In the mean-field (NM) model, the system separates itself in a bulk liquid and gas phase at a transition density or a transition temperature; in the NSE model, the system responds toward the changes by a marked growth of clusters out of the dilute nucleonic gas at a transition point.

The isotherms in the two models look very similar. For symmetric nuclear matter, above the transition density, the pressure remains constant in the density region we study. For asymmetric matter, the pressure increases with density which becomes more prominent with increasing asymmetry. This shows that like the gas-liquid phase transition in the NM model [9], the transition to bulk clusterization in the NSE model for asymmetric matter occurs over a temperature interval implying a continuous transition as opposed to that at constant temperature in the symmetric matter where the transition is first order. This is further manifested in the finite width in c_p or a continuity in S/A for asymmetric nuclear matter whereas for symmetric matter, this is marked by a singularity in c_p or a discontinuity in entropy.

In consonance with the recent experimental indications that the nuclear symmetry energy coefficient of excited fragments produced in a hot nuclear environment gets considerably reduced, calculations have been performed to test the sensitivity of the nuclear EoS with a weakened symmetry energy. Reduction in the symmetry energy induces quantitative changes in both the inclusive and exclusive nuclear observables, but qualitatively their behavior remains similar; overall, an asymmetric matter with weakened symmetry energy coefficient behaves as a regular system of effectively lesser asymmetry.

ACKNOWLEDGMENTS

The authors thank S. Mallick for fruitful discussions. J.N.D. and S.K.S. gratefully acknowledge the financial support from DST and CSIR, Government of India, respectively.

[1] S. E. Koonin and J. Randrup, Nucl. Phys. **A356**, 223 (1981).
[2] J. P. Bondorf, R. Donangelo, I. N. Mishustin, C. J. Pethick, H. Schultz, and K. Sneppen, Nucl. Phys. **A443**, 321 (1985).
[3] D. H. E. Gross, Rep. Prog. Phys. **53**, 605 (1990).
[4] M. F. Rivet *et al*., Phys. Lett. **B388**, 219 (1996).
[5] B. Borderie, J. Phys. G **28**, R217 (2002).
[6] J. Pochodzalla *et al*., Phys. Rev. Lett. **75**, 1040 (1995).
[7] J. Cibor *et al*., Phys. Lett. **B473**, 29 (2000).
[8] J. P. Bondorf *et al*., Phys. Rep. **257**, 133 (1995).
[9] H. Müller and B. D. Serot, Phys. Rev. C **52**, 2072 (1995).
[10] T. Sil, S. K. Samaddar, J. N. De, and S. Shlomo, Phys. Rev. C **69**, 014602 (2004).
[11] K. Huang, *Statistical Mechanics* (Wiley Eastern Ltd., New York, 1986).
[12] R. Dashen, S. K. Ma, and H. J. Bernstein, Phys. Rev. **187**, 345 (1969).
[13] C. J. Horowitz and A. Schwenk, Nucl. Phys. **A776**, 55 (2006).
[14] R. K. Pathria, *Statistical Mechanics*, 1st ed. (Pergamon Press, New York, 1978).
[15] B. S. Meyers, Annu. Rev. Astron. Astrophys. **32**, 153 (1994).
[16] C. Ishizuka, A. Ohnishi, and K. Sumiyoshi, Nucl. Phys. **A723**, 517 (2003).
[17] A. S. Botvina and I. N. Mishustin, Phys. Lett. **B584**, 233 (2004).
[18] A. Le Fevre *et al*., Phys. Rev. Lett. **94**, 162701 (2005).
[19] J. Iglio *et al*., Phys. Rev. C **74**, 024605 (2006).
[20] D. V. Shetty, S. J. Yenello, and G. A. Souliotis, Phys. Rev. C **76**, 024606 (2007).
[21] G. A. Souliotis, A. S. Botvina, D. V. Shetty, A. L. Keksis,

M. Jandel, M. Veselsky, and S. J. Yennello, Phys. Rev. C **75**, 011601(R) (2007).
[22] S. K. Samaddar, J. N. De, X. Viñas, and M. Centelles, arXiv:0706.3385, nucl-th (to be published in Phys. Rev. C, October, 2007).
[23] D. V. Shetty, S. J. Yennello, G. A. Souliotis, A. L. Keksis, S. N. Soisson, B. C. Stein, and S. Wuenschel, arXiv:nucl-ex/0606032, (2006).
[24] A. S. Botvina, N. Buyukcizmeci, M. Erdogan, J. Lukasik, I. N. Mishustin, R. Ogul, and W. Trautmann, Phys. Rev. C **74**, 044609 (2006).
[25] P. Danielewicz, Nucl. Phys. **A727**, 233 (2003).
[26] W. D. Myers and W. J. Swiatecki, Nucl. Phys. **A81**, 1 (1966).
[27] S. Levit and P. Bonche, Nucl. Phys. **A437**, 426 (1985).
[28] K. Kolehmainen, M. Prakash, J. M. Lattimer, and J. Treiner, Nucl. Phys. **A439**, 535 (1985).
[29] J. P. Bondorf, R. Donangelo, I. N. Mishustin, and H. Schultz, Nucl. Phys. **A444**, 460 (1985).
[30] C. B. Das, S. Das Gupta, and A. Z. Mekjian, Phys. Rev. C **68**, 014607 (2003).